

Characterization of Emission Source Localization Accuracy for Bridger Photonics' Gas Mapping LiDAR

1. Abstract

We present test results that characterize the accuracy with which Bridger Photonics, Inc.'s Gas Mapping LiDAR technology determines emission source geodetic coordinates for controlled methane releases under single-blind testing protocols. Testing used standard field-operation data collection and processing procedures and evaluated the uncertainty in geodetic coordinates measured by Gas Mapping LiDAR from an airborne platform relative to real-time-kinematic-calibrated (RTK-calibrated) geodetic coordinates determined on the ground for the same emission sources. Multiple fly-over passes were performed for each sensor unit to generate localization statistics for analysis. For each sensor unit tested, the Gas Mapping LiDAR-measured geodetic coordinates (average geodetic coordinates across all measurements plus one standard deviation) were within 2 m of the calibrated geodetic coordinates. As an indication of overall technology performance across 11 sensors, over 97% of Gas Mapping LiDAR-measured emission source locations were within 2 m of the calibrated geodetic coordinates.

2. Introduction and Motivation

Reducing methane emissions in the oil and gas industry offers a rare win-win for the oil and gas industry and for the environment. Because methane is the principal constituent of natural gas, methane that escapes from oil and gas infrastructure into the atmosphere represents lost product. Reductions and mitigation efforts can increase product brought to market, and therefore increase revenue for oil and gas operators. Additionally, because methane is a potent greenhouse gas,[1] reducing these emissions has been widely identified as an economical and rapid way to mitigate climate change.[2]

To provide the oil and gas industry with effective tools to mitigate methane loss, Bridger Photonics, Inc. (Bridger) developed Gas Mapping LiDAR™ (GML), which was commercialized in 2019. GML images, localizes, and quantifies methane emissions from airborne platforms. GML data is used throughout the natural gas value chain to simplify emissions reduction. To use GML data effectively within emissions management functions, including leak detection and repair programs required by environmental regulations, it is necessary to rigorously characterize technology performance metrics. Previous reports describe GML's detection sensitivity and quantification accuracy,[3,4,5,6,8] this is the first report that explicitly describes the accuracy with which GML can spatially localize emission sources.

For remote sensing technology like GML, the ability to accurately determine a methane emission source location is important because oil and gas operators can use this information to direct their field crews to the location of the problem for repair and mitigation. More accurate localization

(i.e., lower uncertainty in the measured geodetic coordinates of the emission source) can therefore result in more efficient operations. In addition, accurate emission source localization enables emissions to be attributed to equipment classes, which is critical for developing source-resolved emissions inventories,[7] identifying emissions drivers across asset bases, targeting emission types for mitigation, and tracking progress towards emissions reduction goals. The present study compares the geodetic coordinates of controlled release emission sources measured using GML technology to the geodetic coordinates of the same emission sources as determined by real-time-kinematic (RTK) calibration. A sensor qualification metric is described, which requires a sensor to achieve an emission source localization uncertainty of less than 2 m (1σ) across ≥ 12 measurements.

3. Brief Technology Background

The GML sensors used to acquire data for this study use the absorption of laser light to detect, localize, and quantify methane gas. GML scans an eye-safe laser beam across the ground surface from an aircraft to produce path-integrated methane gas concentration imagery. Bridger also acquires topographical LiDAR to accurately determine the distance to the ground surface for ambient methane background subtraction and to assist with spatial geo-location within internal data processing. The acquired GML data is geo-registered to the ground surface using on-board GPS, inertial measurement unit (IMU), beam scanner encoder, and LiDAR range measurements. RGB digital camera images are concurrently acquired with LiDAR data to provide contextual information for emission sources and for other informatics on scan regions. For the production sector, GML has demonstrated an average and median detection sensitivity of less than 2 kg/hr (104 scfh) with 90% probability of detection (POD) in every major oil and gas production basin in the US and Canada.[6,8,9,10]

4. Description of Experiment and Setup

In the present study, comparisons were performed between the calibrated geodetic coordinates of a controlled release emission sources ("emission source location") with the geodetic coordinates of the same emission source as measured by GML under standard field operational conditions. The GML coordinates were determined without knowledge of where the emission source was located within the test area or knowledge of the controlled emission rate. Controlled release emission rates were varied during the testing to simulate more realistic conditions. Wind measurements were performed using anemometers during the testing to document the wind speed conditions. The wind speed data is not used to locate emission sources, but it is necessary for determining suitable controlled release emission rates and methane plume development periods. In addition, wind speed data is used for other aspects of sensor evaluation that are outside the scope of the present study.

Figure 1 shows an image of a typical controlled release site used to qualify Bridger's GML sensors. The controlled release site includes a metered methane emission source mounted at a height above ground level (AGL) of 1.8 m, and three anemometers mounted at 1.8 m AGL (one three-cup anemometer and two ultrasonic anemometers). Each test site footprint is at least 100 m x 100 m and the emission source was positioned within the site footprint at the start of each testing day. As illustrated by Figure 1, the emission source was positioned away from significant topographical features, structures, and foliage that might disturb local wind fields. To allow each

new methane plume adequate time to develop for independent measurements, a minimum time delay of approximately 90 seconds between subsequent flyover passes was enforced. Fully vs. partially- (or "undeveloped") plumes were determined according to the protocol described in Reference 6.

The emission source location for each controlled release measurement was calibrated using a Trimble AP15 paired with a Trimble AV39 antenna, providing a geodetic coordinate (latitude and longitude) uncertainty of no greater than 20 cm (standard accuracy). For some testing, the location system was upgraded to a Trimble DA2, providing measurement uncertainty as low as 1 cm (high accuracy).

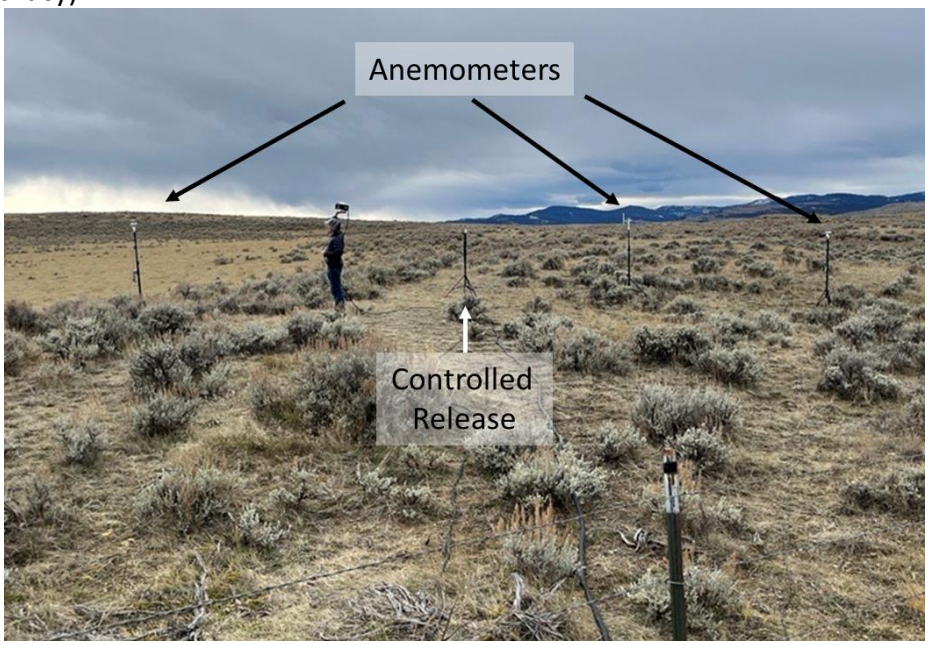

Figure 1. A typical controlled release site. The emission source is pseudo-randomly placed each testing day, and anemometers are placed around the emission source.

Figure 2 shows Bridger's mobile controlled release test station. The test station van is equipped with multiple k-bottles, high and low flow rate gas flow controllers, and a data logger to record the wind and flow data at one-second intervals. Running 30-second averages are performed for calculating wind speeds and metered gas flow rates.

Figure 2. Bridger's mobile controlled release test station.

Testing was performed with GML sensors mounted to the wing strut of a Cessna 172 aircraft. The testing of each sensor in this study comprised at least 25 scans of the controlled release site. Fifteen scans were performed from 700' AGL and 10 scans were performed at 500' AGL to collect data corresponding to different operating parameters. The aircraft was flown at approximately 90 mph (~78 knots). The flight passes alternated in orthogonal directions north -> south, west -> east, north -> south, etc.

Testing was performed using a range of metered flow rates for which GML has differing expected plume detection probabilities. Table 1 shows the targeted probability of detection (PoD) for the controlled releases, based on anticipated factors including flight altitude, ground reflectivity, and measured wind speed. Release rates for each measurement were selected pseudo-randomly. Testing used single-blind testing protocols, meaning that the metered flow rate and emission source location were not disclosed for data acquisition or processing.

Table 1. The targeted probability of detection values for the controlled release tests.

Number of Releases	Probability of Detection
2	10%
2	30%
2	50%
1	70%
2	80%
3	85%
5	90%
3	95%
5	99+%

5. Description of Data Processing Protocols

Raw sensor data was processed using GML's standard automated routine to determine the locations and extents of regions of elevated methane concentration (i.e., methane plumes) using

a statistical algorithm similar to that described in Reference 11. The algorithm applies an adaptive gas concentration threshold to identify methane plumes relative to background gas concentrations while using gas concentration noise models to account for variable levels of measurement noise. The automated plume detection processing in this study used the same algorithm and calibration parameters as commercial GML scans, thereby eliminating bias or subjectivity in plume detections. Data for processing was selected using a geospatial polygon feature that enclosed the test site. Figure 3 shows a Google Earth image of the 4 January 2024 test site. The controlled release polygon feature and a GML camera image are overlaid for reference.

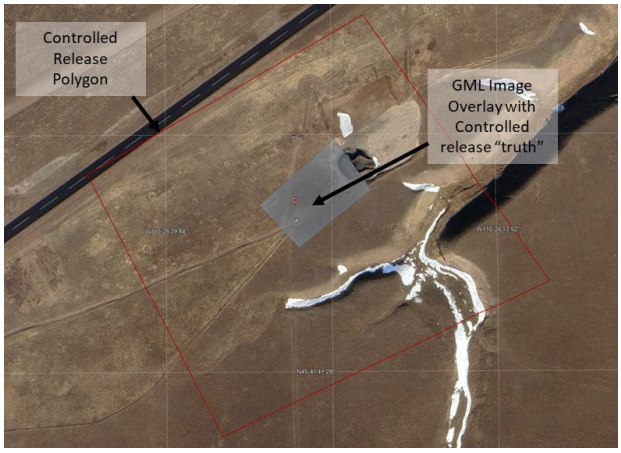

Figure 3. A Google Earth image of the 4 January 2024 test site. The controlled release site polygon feature and a GML camera image are overlaid for reference.

After the automated processing step, Bridger's data processing personnel use a custom software application and the same information and protocols as a typical commercial GML flight to assign emission source locations to the detected methane plume data. The emission source location is assigned without access to the geodetic coordinates of the emission source. First, the plume height is determined. Next, the underlying topographic LiDAR point cloud data, colored by the signal-to-noise ratio of the path-integrated gas concentration for each LiDAR measurement point is analyzed to determine if an emission source location can be assigned. The threshold for assigning an emission source location to a detected methane plume is three or more adjacent LiDAR points with path-integrated gas concentration signal-to-noise ratio exceeding a fixed threshold. The threshold value used during sensor testing is identical to the threshold used for commercial operations. Detection events, along with flyover time, measured emission source location geodetic coordinates, and wind speed at the measured plume height are compiled into a report. Figure 4 shows a Google Earth image of the 4 January 2024 test site with a methane plume image and GML camera image from senor testing overlaid on an image from Google Earth.

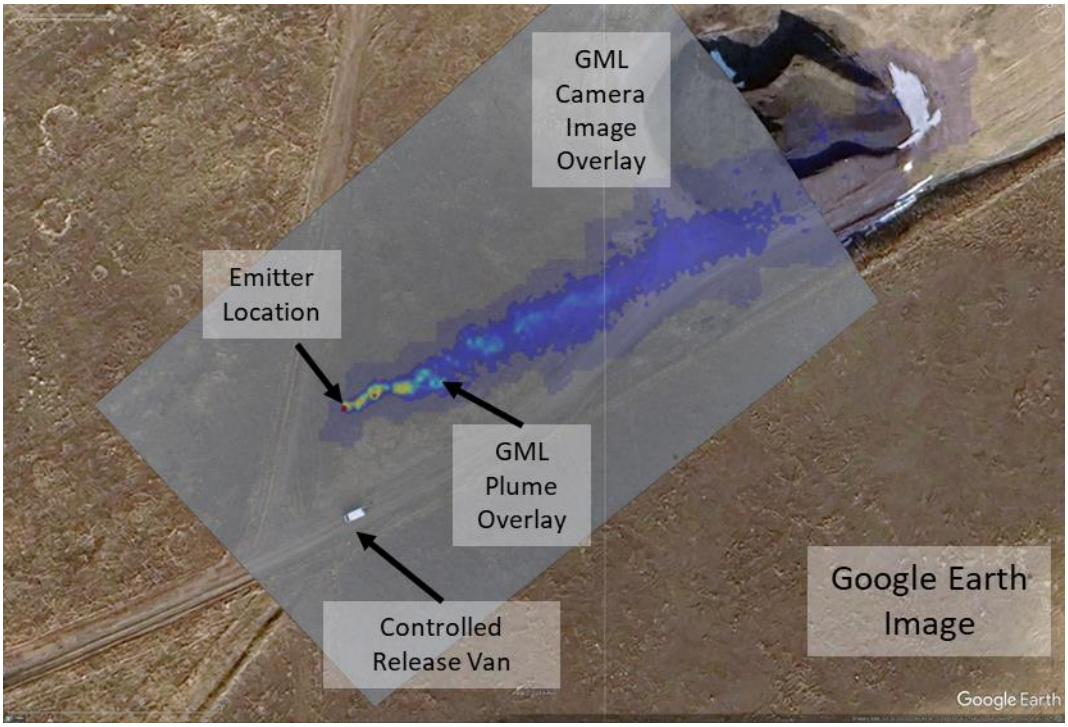

Figure 4. Imagery from testing at the 4 January 2024 test site. A GML camera image and a methane gas plume image from sensor testing are overlaid on a Google Earth image.

6. Description Results

Data acquired during GML controlled release testing was processed using Bridger's standard work practice. GML-measured emission source locations from controlled release test data were compared to emission source locations determined at the testing site using the Trimble DA2 (high accuracy) instrument which was treated as the "true" value for locations. Figure 5 shows measured GML emission source location errors. The latitude/longitude for detections and truth are converted into local geodetic coordinates and a location error in Cartesian coordinates is calculated for each detection.

For each sensor testing program, the pass/fail metric requires that the GML-measured geodetic coordinates (average plus one standard deviation for at least 12 independent measurements) for an emission source is within 2 m of the actual emission source location. Each measured emission source location relative to the true emission source location is indicated in Figure 5 by a blue filled (empty) circle for fully (partially) developed plumes. The mean position is indicated by a black filled circle. One standard deviation away from the average location measurement is shown with the dashed black ovals. The 2-m pass/fail specification is shown as dashed red circles.

The GML emission source location measurements presented in Figure 5 are all located within 2 m of the "true" location, and the 1 standard deviation rings are well within the 2-m pass / fail rings. A more exhaustive dataset using both high-accuracy and standard accuracy global positioning systems to assign "true" emission source locations is shown in Figure 6. This dataset covers 11 sensor testing programs, representing 321 individual measurements. Data from testing individual sensors are represented by different markers. Notice more than 97% of the measurements fall within the 2-m pass / fail ring. The right figure shows the mean and range of

the absolute errors for each sensor. The data was collected for both fully and partially developed plumes over a wide range of wind-speeds and controlled release rates as shown in Figure 7. Each of the 11 sensors tested passed the localization performance qualification metric.

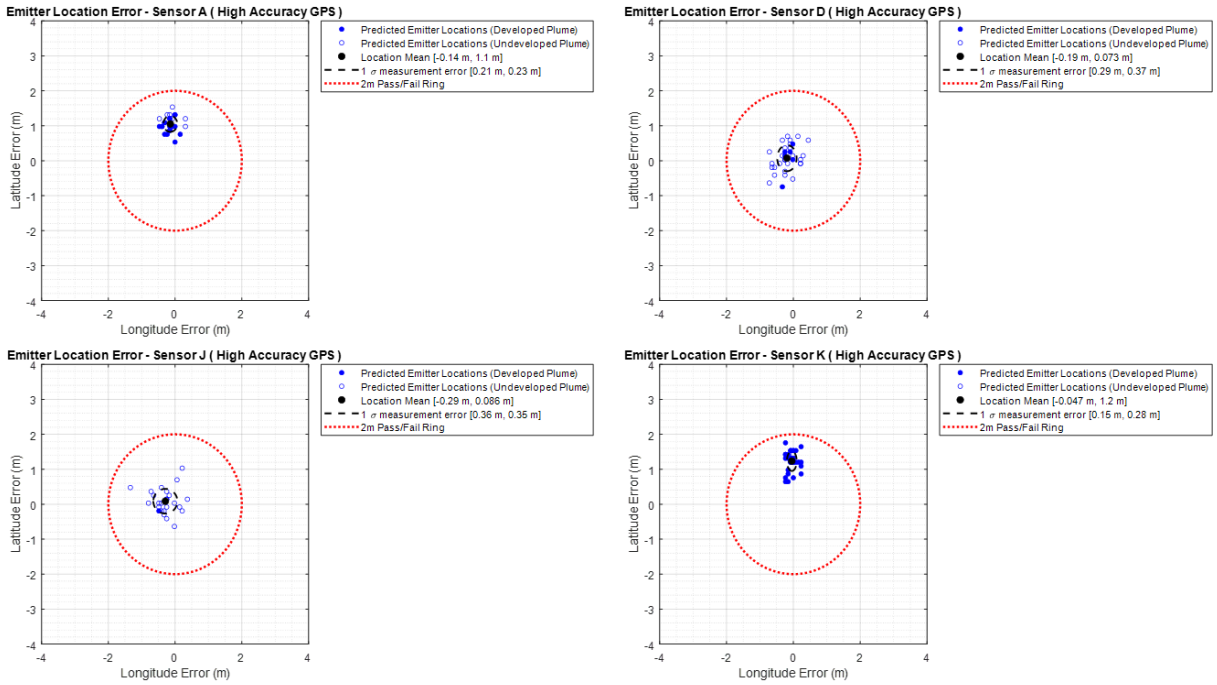

Figure 5. GML emission source location measurement errors for individual sensor testing programs using the Trimble DA2 (high accuracy) to provide a "truth." The solid circles show results for fully developed plumes and the open circles show results for partially developed plumes.

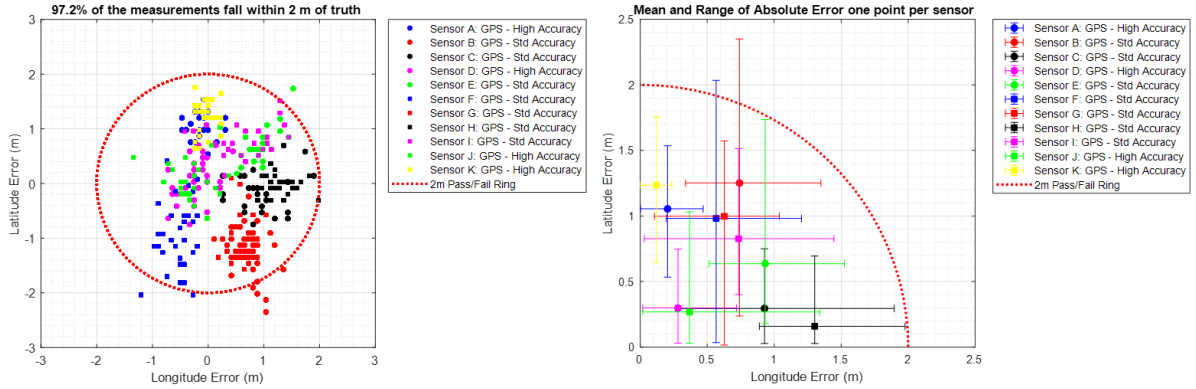

Figure 6. GML emission source location measurement errors during qualification testing of 11 sensors. There were a total of 321 emission source location measurements during testing for this sensor cohort. The left figure shows location errors for all sensors, with more than 97% of the measurements falling within 2 m of the "true" emission source location. The right figure shows the mean error for each sensor and the range of absolute error in longitude and latitude for that sensor.

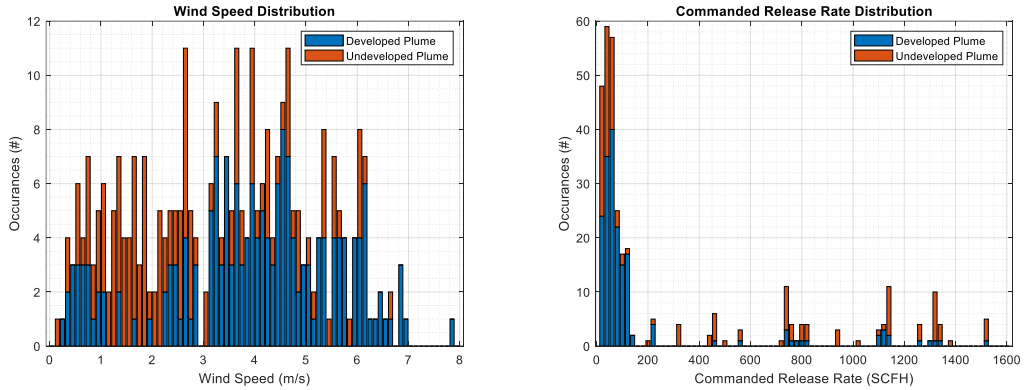

Figure 7. The left figure shows the wind speed distribution for the 321 detection events within testing programs for 11 GML sensors. The right figure shows the commanded release rate distribution for the detections.

7. Summary and Conclusions

This study presented experiments and analysis to assess the accuracy with which Bridger's GML technology measures the geodetic coordinates of controlled release emission source locations under non-turbulent wind conditions. For each GML sensor unit tested, the measured geodetic coordinates met Bridger's localization qualification metric that the average localization value plus one standard deviation must be within 2 m of the true emission source location. Testing covered a range of controlled release rates over varying wind conditions. For 11 sensors and 321 detection events, over 97% of GML-measured source locations were within 2 m of the calibrated geodetic coordinates of the controlled release emission sources.

The reported test results provide a robust characterization of GML sensor localization capabilities for methane plumes in simple wind fields. The translation of test results to identifying emission source locations of operational oil and gas infrastructure is demonstrated in peer reviewed literature, where ground crews using OGI cameras were able to attribute causes to 192 out 195 emission sources identified by GML, with the follow-up for the remaining 3 detections being hindered by confusion on site orientation or by high winds.[12]

Contact: Info at 406.522.3766 or info@bridgerphotonics.com

References

[1] Szopa, S.; Naik, V.; Adhikary, P.; Berntsen, T.; Collins, W.D.; Fuzzi, S.; Gallardo, A.; Kiendler-Scharr, Z.; Klimont, H.; Liao, N.; Under, N.; Zanis, P. Chapter Short-lived Climate Forcers. In Climate Change 2021: The Physical Science Basis. Contribution of Working Group I to the Sixth Assessment Report of the Intergovernmental Panel on Climate Change; Masson-Delmotte, V., Zhai, P.; Pirani, A.; Connors, S. L.; Pean, C.; Berger, S.; Caud, N.; Chen, Y.; Goldfarb, L.; Gomis, M.I.; Huang, M.; Leitzell, K.; Lonnoy, E.; Matthews, J.B.R.; Maycock, T. K.; Waterfield, T.; Yelekci, O.; Yu, R.; Zhao, B.; Eds. Cambridge University Press, 2021; pp817−922, see Figure 6.16.
[2] White House. U.S. Methane Emissions Reduction Action Plan; 2021.
[3] Bridger Photonics, Inc. Performance of Gas Mapping LiDAR™ for Quantification of Very High Methane Emission Rates; 2021.
[4] Bell, C.; Rutherford, J.; Brandt, A.; Sherwin, E.; Vaughn, T.; Zimmerle, D. Single-Blind Determination of Methane Detection Limits and Quantification Accuracy Using Aircraft-Based LiDAR. Elementa: Science of the Anthropocene 2022, 10 (1), 00080. https://doi.org/10.1525/elementa.2022.00080.

[5] Conrad, B. M.; Tyner, D. R.; Johnson, M. R. Robust Probabilities of Detection and Quantification Uncertainty for Aerial Methane Detection: Examples for Three Airborne Technologies. Remote Sensing of Environment 2023, 288, 113499. https://doi.org/10.1016/j.rse.2023.113499.
[6] Thorpe, M.; Krietinger, A.; Altamura, D.; Dudiak, C.; Conrad, B.; Tyner, D.; Johnson, M.; Brasseur, J.; Roos, P.; Kunkel, W.; Carre-Burritt, A.; Abate, J.; Price, T.; Yaralian, D.; Kennedy, B.; Newton, E.; Rodriguez, E.; Ibrahim Elfar, O.; Zimmerle, D. Deployment-Invariant Probability of Detection Characterization for Aerial LiDAR Methane Detection; preprint; *Environmental Monitoring*, 2024. https://doi.org/10.31223/X5R96M.
[7] Johnson, M. R.; Conrad, B. M.; Tyner, D. R. Creating Measurement-Based Oil and Gas Sector Methane Inventories Using Source-Resolved Aerial Surveys. *Communications Earth & Environment* 2023, 4 (1), 139. https://doi.org/10.1038/s43247-023-00769-7.
[8] Matthew R. Johnson, David R.Tyner, and Alexander J.Szekeres, "Blinded evaluation of airborne methane source detection using Bridger Photonics LiDAR," *Remote Sensing of Environment* 2021 259, *112418*. https://doi.org/10.1016/j.rse.2021.112418
[9] David R. Tyner and Matthew R. Johnson, "Where the Methane Is—Insights from Novel Airborne LiDAR Measurements Combined with Ground Survey Data," *Environmental Science & Technology* 2021 55 (14), 9773-9783. DOI: 10.1021/acs.est.1c01572
[10] Collaboratory to Advance Methane Science – Scientific Insights, "Permian Basin Survey: An array of aerial surveys in the Permian Basin to acquire the baseline distribution of methane emission rates and sources," https://methanecollaboratory.com/wp-content/uploads/2021/08/Scientific-Insights-Aerial-Survey-in-Permian-August2021_vFinal.pdf
[11] Kreitinger, A. T.; Thorpe, M. J. APPARATUSES AND METHODS FOR ANOMALOUS GAS CONCENTRATION DETECTION. WO-US-01 11112308 **2021**
[12] Johnson, M. R.; Tyner, D. R.; Conrad, B. M. Origins of Oil and Gas Sector Methane Emissions: On-Site Investigations of Aerial Measured Sources. *Environmental Science & Technology* 2023, 57 (6), 2484–2494. https://doi.org/10.1021/acs.est.2c07318.